DOR: 20.1001.1.27170314.2022.11.1.3.9

Research Paper

Assessment of Third-order Shear Deformation Graphene Nanoplate Response under Static Loading Using Modified Couple Stress Theory

Majid Eskandari Shahraki[1], Mahmoud Shariati[1*], Naser Asiaban[1], Ali Davar[2], Mohsen Heydari Beni[2], Jafar Eskandari Jam[2]

[1]Faculty of Engineering, Ferdowsi University of Mashhad, Mashhad, Iran

[2]Faculty of Materials and Manufacturing Technologies, Malek Ashtar University of Technology, Tehran, Iran

[*]Email of Corresponding Author: mshariati44@um.ac.ir

Received: March 22, 2022; Accepted: May 9, 2022

Abstract

In this paper bending and buckling characteristics of third-order shear, and deformation nanoplates were investigated using the modified couple stress theory and Navier type solution. It can be useful for designing and manufacturing micro-electromechanical and nano-electromechanical systems. The modified couple stress theory was applied to provide the possibility of considering the effects of small scales that have only one material length scale parameter. In this theory, the strain energy density is a function of the strain tensor components, curvature tensor, stress tensor, and the symmetric part of the couple stress tensor. After obtaining the strain energy, external work, and buckling equations, the Hamilton principle is employed to derive the governing equations. Furthermore, by applying boundary and loading conditions in the governing equations, the bending and buckling of a third-order shear deformation nanoplate with simply-supported bearings are obtained and the Navier's solution is used to solve the equations. The results indicate that the third-order nanoplate subjected to sinusoidal loading yields smaller values of dimensionless bending than it does while subjected to uniform surface traction. It was also found that by increasing the length to thickness ratio, the value of the dimensionless bending of nanoplate decreases but by increasing the aspect ratio of the plate, this value increases. Furthermore, it was shown that the critical buckling load of the third-order nanoplate under uniaxial loading increases by increasing the ratio of the length scale parameter to the thickness of the nanoplate but it decreases by increasing the length to thickness ratio of the nanoplate.

Keyword

Modified Couple-stress Theory, Third-order Nano-plate, Navier Solution Method, Bending, Buckling

1. Introduction

Performing experiments on the atomic and molecular scales are the safest approach for the study of materials on small scales that causes a real dimensions investigation on the structures. To determine the mechanical properties of nanostructures in this method, various mechanical loads are applied to nanostructures using atomic Force Microscopy (AFM) and the plate responses are measured. The difficulties of controlling the test conditions at this scale, high economic costs, and time-consuming processes are some setbacks of this approach. Therefore, it is only used to validate other simple and

low-cost methods.

Atomic simulation is another approach for studying small-scale structures. In this method, the behaviors of atoms and molecules are examined by considering the intermolecular and interatomic effects on their motions, which ultimately involves the total deformation of the body. In the case of large deformations and multi atomic scales, the computational costs of this approach become unbearable, so it is only used for small deformation problems.

Given the limitations of the aforementioned methods for the study of small scales, the literature was directed toward finding more efficient solutions which are reliable and less costly, and time-consuming. Modeling small-scale structures using continuum mechanics is one of these solutions. There are a variety of size-dependent continuum theories that consider size effects and are suitable for this problem. Some of these theories are; the micromorphic theory, microstructural theory, micropolar theory, Kurt's theory, non-local theory, modified couple stress theory, and strain gradient elasticity.

Thanh et al, [1] studied the size-dependent thermal bending and buckling responses of composite laminate microplate-based on a new modified couple stress theory and isogeometric analysis. The influences of fiber orientation, thickness ratio, boundary conditions, and the variation in material length scale parameter were also investigated.

Sladek et al, [2] studied the FGM micro/nano-plates within modified couple stress elasticity. The boundary restrictions on the bottom and top surfaces of the plate together with the derivation of governing equations and physical boundary conditions on the plate edges were investigated and discussed in detail

Al-Shewailiah et al, [3] studied the static bending of functionally graded single-walled carbon nanotube in conjunction with modified couple stress theory. The characteristics which were investigated, include length, material parameter ratio, and the volume fraction of material, porosity and carbon nanotube, SWCNT distribution types, boundary conditions, and aspect ratio (length/thickness). By observing the static behavior of FG-micro beams it was found that the modified couple stress theory (MCST) yields more accurate results than classical beams.

Yang et al, [4] studied the axisymmetric bending and vibration of circular nanoplates with surface tractions. They investigated the effect of the material's surface properties on deflection and natural frequencies.

Aghababaei and Reddy, [5] employed the non-local third-order shear deformation plate theory to study the bending and vibration of plates. They presented Eringen’s analytical solution for bending and free vibration of a simply supported rectangular plate using non-local linear elasticity theory to illustrate the effect of non-local theory on deflection and natural frequency of the plates.

Jung et al, [6] studied the buckling of S-FGM nanoplates embedded in Pasternak elastic medium using a modified couple stress theory. The effects of the power-law index, small-scale coefficient, aspect ratio, side-to-thickness ratio, loading types, and elastic medium parameter on the buckling load of S-FGM nanoplates were also investigated.

Shafiei et al, [7] employed the modified couple stress theory to study the stability and vibration of single and multi-layered graphene sheets. The effects of different parameters such as loading schemes, nanoplate dimensions, and boundary conditions were investigated.

Wu et al. [8] studied a unified size-dependent plate theory for static bending and vibration analyses of micro and nano-scale plates based on the consistent couple stress theory. They observed that the material length scale parameter effects on static bending and free vibration behaviors of the FGMP/MLGS are significant.

Haghshenas and Shahrajabian [9] studied the Mechanical Properties of PA6/NBR/clay/CaCO3 Hybrid Nanocomposites. They evaluated mechanical properties by tensile, flexural, and Charpy impact tests. The results showed that adding the NBR reduces the tensile strength, tensile modulus, flexural strength, and flexural modulus and increases the impact strength.

Graphene is an intelligent material that exhibits excellent properties used for various industrial applications such as High-speed electronics, Data storage, LCD smart windows, OLED displays, Supercapacitors, Solar cells/photovoltaic cells, Thermoelectric applications, Shape memory materials, Self-healing materials, and Electrorheology materials[10].

Nanoelectromechanical systems (NEMS) are the logical miniaturization step of so-called microelectromechanical systems (MEMS). Due to the special properties of integrating electrical and mechanical functionality on the nanoscale, NEMS will play an important role in the future of computing and sensing fields. When the size of the resonator reaches about 100 nm, NEMS can be operated at a high frequency, which can be up to 1 GHz, and provide extreme sensitivity. At present, Si and GaAs are widely used in NEMS, which have a high Young's modulus (>~100 GPa) and can be easily fabricated into complicated planar structures. However, Si and GaAs cannot satisfy the needs of NEMS.

So, it is of great significance to acquire materials with low density and high Young's modulus for the fabrication of NEMS. Among the nanomaterials, carbon-based nanomaterials such as diamond, carbon nanotube, and graphene have high ratios of Young's modulus to density, and graphene is of great attention for its special properties such as portable quality, ultra hardness, excellent Young's modulus, high thermal conductivity, and the high surface area-to-volume ratio[11]. Therefore graphene nanoplates can be substituted for silicon as a load-bearing material.

Accordingly, the study of the critical buckling and bending load of nanoplates can be useful for designing and manufacturing micro-electromechanical and nano-electromechanical systems.

In this paper, a third-order shear deformation nanoplate model is developed for bending and buckling analysis of a graphene nanoplate based on the modified couple stress theory. The results are presented in figures and tables and are discussed in detail.

2. Methods

2.1 Modified couple stress theory

Yang et al. [12] proposed a modified couple stress model by modifying the theory proposed by Toppin [13], Mindlin and Thursten [14], Quitter [15], and Mindlin [16] in 1964. The modified couple stress theory consists of only one material length scale parameter for the projection of the size effect, whereas the classical couple stress theory needs two material length scale parameters. In the modified theory the strain energy density for a body bounded by the volume V and the area Ω [17], is expressed as follows:

$$U = \frac{1}{2}\int_V \left(\sigma_{ij}\varepsilon_{ij} + m_{ij}\chi_{ij}\right)dV \quad i,j = 1,2,3 \tag{1}$$

Where:

$$\varepsilon_{ij} = \frac{1}{2}(u_{i,j} + u_{j,i}) \quad (2)$$

$$\chi_{ij} = \frac{1}{2}(\theta_{i,j} + \theta_{j,i}) \quad (3)$$

Where χ_{ij} and ε_{ij} are symmetric parts of the curvature tensor and strain tensors, respectively. Also, u_i and θ_i are defined as displacement and rotation vectors, respectively.

$$\theta = \frac{1}{2}\, Curl\, \boldsymbol{u} \quad (4)$$

σ_{ij}, the stress tensor, and $m_{i,j}$, the deviatory part of the couple stress tensor, is defined as:

$$\sigma_{ij} = \lambda \varepsilon_{kk}\delta_{ij} + 2\mu\varepsilon_{ij} \quad (5)$$

$$m_{i,j} = 2\mu\, l^2 \chi_{ij} \quad (6)$$

Where λ and μ are the lame constants, δ_{ij} is the Kronecker delta and l is the material length scale parameter. From Eq. (3) and (6) it can be seen that χ_{ij} and m_{ij} are symmetric.

2.2 Third-order plate model

The displacement equations for the third-order plate are defined as follows:

$$u_1(x,y,z) = z\,\varphi_x(x,y) - \frac{4}{3}\left(\frac{1}{h}\right)^2 z^3\left(\frac{\partial w(x,y)}{\partial x} + \varphi_x(x,y)\right) \quad (7)$$

$$u_2(x,y,z) = z\varphi_y(x,y) - \frac{4}{3}\left(\frac{1}{h}\right)^2 z^3\left(\frac{\partial w(x,y)}{\partial y} + \varphi_y(x,y)\right)$$

$$u_3(x,y,z) = w(x,y)$$

Where φ_x and φ_y are the rotations of the normal vector around the x and y-axis respectively, and w is the midpoint displacement of the plate in the z-axis direction. The strain and stress tensors, the symmetric part of the curvature tensor, and the rotational vector for the nth-order plate are obtained as follows:

$$\varepsilon_{xx} = z\frac{\partial \varphi_x}{\partial x} - \frac{4}{3}\left(\frac{1}{h}\right)^2 z^3\left(\frac{\partial^2 w}{\partial x^2} + \frac{\partial \varphi_x}{\partial x}\right) \quad (8)$$

$$\varepsilon_{yy} = z\frac{\partial \varphi_y}{\partial y} - \frac{4}{3}\left(\frac{1}{h}\right)^2 z^3\left(\frac{\partial^2 w}{\partial y^2} + \frac{\partial \varphi_y}{\partial y}\right) \quad (9)$$

$$\varepsilon_{zz} = 0 \quad (10)$$

$$\varepsilon_{xy} = \varepsilon_{yx} = \frac{1}{2}z\left(\frac{\partial \varphi_x}{\partial y} + \frac{\partial \varphi_y}{\partial x}\right) - \frac{2}{3}\left(\frac{1}{h}\right)^2 z^3\left(\frac{\partial \varphi_x}{\partial y} + \frac{\partial \varphi_y}{\partial x} + 2\frac{\partial^2 w}{\partial x \partial y}\right) \quad (11)$$

$$\varepsilon_{xz} = \varepsilon_{zx} = \left(\frac{1}{2} - 2\left(\frac{z}{h}\right)^2\right)\left(\frac{\partial w}{\partial x} + \varphi_x\right) \quad (12)$$

$$\varepsilon_{yz} = \varepsilon_{zy} = \left(\frac{1}{2} - 2\left(\frac{z}{h}\right)^2\right)\left(\frac{\partial w}{\partial y} + \varphi_y\right) \quad (13)$$

$$\theta_x = \frac{\partial w}{\partial y} - \left(\frac{1}{2} - 2\left(\frac{z}{h}\right)^2\right)\left(\frac{\partial w}{\partial y} + \varphi_y\right) \quad (14)$$

$$\theta_y = -\frac{\partial w}{\partial x} + \left(\frac{1}{2} - 2\left(\frac{z}{h}\right)^2\right)\left(\frac{\partial w}{\partial x} + \varphi_x\right) \quad (15)$$

$$\theta_z = \frac{1}{2}\left(z - \frac{4}{3}\left(\frac{1}{h}\right)^2 z^3\right)\left(\frac{\partial \varphi_y}{\partial x} - \frac{\partial \varphi_x}{\partial y}\right) \quad (16)$$

$$x_{xx} = \frac{\partial^2 w}{\partial x\,\partial y} - \left(\frac{1}{2} - 2\left(\frac{z}{h}\right)^2\right)\left(\frac{\partial^2 w}{\partial x\,\partial y} + \frac{\partial \varphi_y}{\partial x}\right) \quad (17)$$

$$x_{yy} = -\frac{\partial^2 w}{\partial x \partial y} + \left(\frac{1}{2} - 2\left(\frac{z}{h}\right)^2\right)\left(\frac{\partial \varphi_x}{\partial y} + \frac{\partial^2 w}{\partial x \partial y}\right) \quad (18)$$

$$x_{zz} = \left(\frac{1}{2} - 2\left(\frac{z}{h}\right)^2\right)\left(\frac{\partial \varphi_y}{\partial x} - \frac{\partial \varphi_x}{\partial y}\right) \quad (19)$$

$$x_{xy} = \frac{1}{2}\left(\frac{\partial^2 w}{\partial y^2} - \frac{\partial^2 w}{\partial x^2}\right) + \left(\frac{1}{4} - \left(\frac{z}{h}\right)^2\right)\left(\frac{\partial^2 w}{\partial x^2} + \frac{\partial \varphi_x}{\partial x} - \frac{\partial^2 w}{\partial y^2} - \frac{\partial \varphi_y}{\partial y}\right) \quad (20)$$

$$x_{xz} = \frac{1}{4}\left(z - \frac{4}{3}\left(\frac{1}{h}\right)^2 z^3\right)\left(\frac{\partial^2 \varphi_y}{\partial x^2} - \frac{\partial^2 \varphi_x}{\partial y\,\partial x}\right) + 2z\left(\frac{1}{h}\right)^2\left(\frac{\partial w}{\partial y} + \varphi_y\right) \quad (21)$$

$$x_{yz} = -2z\left(\frac{1}{h}\right)^2\left(\frac{\partial w}{\partial x} + \varphi_x\right) + \frac{1}{4}\left(z - \frac{4}{3}\left(\frac{1}{h}\right)^2 z^3\right)\left(\frac{\partial^2 \varphi_y}{\partial x \partial y} - \frac{\partial^2 \varphi_x}{\partial y^2}\right) \quad (22)$$

$$\sigma_{xx} = (\lambda + 2\mu)\mathcal{E}_{xx} + \lambda\mathcal{E}_{yy} \quad (23)$$

$$\sigma_{yy} = \lambda\mathcal{E}_{xx} + (\lambda + 2\mu)\mathcal{E}_{yy} \quad (24)$$

$$\sigma_{zz} = \lambda\left(\mathcal{E}_{xx} + \mathcal{E}_{yy}\right) \quad (25)$$

$$\sigma_{yx} = \sigma_{xy} = 2\mu\,\mathcal{E}_{xy} \quad (26)$$

$$\sigma_{xz} = \sigma_{zx} = 2\mu\,\mathcal{E}_{xz} \quad (27)$$

$$\sigma_{yz} = \sigma_{zy} = 2\mu\,\mathcal{E}_{yz} \quad (28)$$

The variation of strain energy is expressed as follows:

$$\delta U = \int_V \sigma_{xx}\,\delta\,\mathcal{E}_{xx} + \sigma_{yy}\,\delta\mathcal{E}_{yy} + 2\sigma_{xy}\,\delta\,\mathcal{E}_{xy} + 2\sigma_{xz}\,\delta\,\mathcal{E}_{xz} + 2\sigma_{yz}\,\delta\,\mathcal{E}_{yz} + m_{xx}\,\delta\,x_{xx} + m_{yy}\,\delta x_{yy} + m_{zz}\,\delta x_{zz} + 2m_{xy}\,\delta x_{xy} + 2m_{xz}\,\delta x_{xz} + 2m_{yz}\,\delta\,x_{yz})dV \quad (29)$$

For the sake of simplification, the coefficient of each variable in the above equation is named from E_1 to E_{15} and this equation can be rewritten as shown below:

$$\delta U = \int_V (E_1\delta w_{,xx} + E_2\,\delta w_{,yy} + E_3\,\delta w_{,xy} + E_4\delta\,w_{,x} + E_5\,\delta\,w_{,y} + E_6\,\delta\,\varphi_{x,yy} + E_7\delta\,\varphi_{y,xx} + E_8\,\delta\,\varphi_{y,xy} + E_9\,\delta\varphi_{x,yx} + E_{10}\,\delta\,\varphi_{x,x} + E_{11}\,\delta\varphi_{y,y} + E_{12}\delta\varphi_{x,y} + E_{13}\,\delta\,\varphi_{y,x} + E_{14}\,\delta\varphi_x + E_{15}\,\delta\varphi_y)dV \quad (30)$$

Where E_1 to E_{15} are calculated as shown:

$$E_1 = \frac{\partial^2 w}{\partial x^2}\left[(\lambda+2\mu)(C_3 - C_1C_2) + \frac{1}{2}\mu l^2(1+C_4) - \frac{1}{4}\mu l^2(1+C_4)(1-C_4)\right] + \frac{\partial^2 w}{\partial y^2}\left[\lambda(C_3 - C_1C_2) - \frac{1}{2}\mu l^2(1+C_4) + \frac{1}{4}\mu l^2(1-C_4)(1+C_4)\right] + \frac{\partial \varphi_x}{\partial x}\left[-(\lambda+2\mu)(C_2C_1) - \frac{1}{4}\mu l^2(1-C_4)(1+C_4)\right] + \frac{\partial \varphi_y}{\partial y}\left[-\lambda(C_2C_1) - \frac{1}{4}\mu l^2(1-C_4)(1+C_4)\right] \quad (31)$$

$$\begin{aligned} E_2 = \frac{\partial^2 w}{\partial y^2}&\left[(\lambda+2\mu)(C_3 - C_1C_2) + \frac{1}{2}\mu l^2(1+C_4)\right. \\ &\left. - \frac{1}{4}\mu l^2(1+C_4)(1-C_4)\right] \\ &+ \frac{\partial^2 w}{\partial x^2}\left[\lambda(C_3 - C_1C_2) - \frac{1}{2}\mu l^2(1+C_4)\right. \\ &\left. + \frac{1}{4}\mu l^2(1-C_4)(1+C_4)\right] \\ &+ \frac{\partial \varphi_y}{\partial y}\left[-(\lambda+2\mu)(C_2C_1) - \frac{1}{4}\mu l^2(1-C_4)(1+C_4)\right] \\ &+ \frac{\partial \varphi_x}{\partial x}\left[-\lambda(C_2C_1) - \frac{1}{4}\mu l^2(1-C_4)(1+C_4)\right] \end{aligned} \quad (32)$$

$$E_3 = \frac{\partial^2 w}{\partial x\,\partial y}\left[4\mu\,{C_2}^2 + \mu l^2(1+C_4)^2\right] + \frac{\partial \varphi_x}{\partial y}\left[-2\mu C_2C_1 - \frac{1}{2}\mu l^2(1-C_4)(1+C_4)\right] + \frac{\partial \varphi_y}{\partial x}\left[-2\mu C_2C_1 - \frac{1}{2}\mu l^2(1-C_4)(1+C_4)\right] \quad (33)$$

$$E_4 = \left(\frac{\partial w}{\partial x} + \varphi_x\right)\left[\mu(1-C_4)^2 + \frac{1}{4}\mu l^2{C_5}^2\right] + \left(\frac{\partial^2 \varphi_y}{\partial x \partial y} - \frac{\partial^2 \varphi_x}{\partial y^2}\right)\left[\frac{1}{4}\mu l^2 C_5C_1\right] \quad (34)$$

$$E_5 = \left(\frac{\partial w}{\partial y} + \varphi_y\right)\left[\mu(1-C_4)^2 + \frac{1}{4}\mu l^2{C_5}^2\right] + \left(\frac{\partial^2 \varphi_x}{\partial x \partial y} - \frac{\partial^2 \varphi_y}{\partial x^2}\right)\left[\frac{1}{4}\mu l^2 C_5C_1\right] \quad (35)$$

$$E_6 = E_8 = \left(\frac{\partial w}{\partial x} + \varphi_x\right)\left[\frac{1}{4}\mu l^2 C_5C_1\right] + \left(\frac{\partial^2 \varphi_y}{\partial x \partial y} - \frac{\partial^2 \varphi_x}{\partial y^2}\right)\left[\frac{1}{4}\mu l^2{C_1}^2\right] \quad (36)$$

$$E_7 = E_9 = \left(\frac{\partial w}{\partial y} + \varphi_y\right)\left[-\frac{1}{4}\mu l^2 C_5C_1\right] + \left(\frac{\partial^2 \varphi_y}{\partial x^2} - \frac{\partial^2 \varphi_x}{\partial x \partial y}\right)\left[\frac{1}{4}\mu l^2{C_1}^2\right] \quad (37)$$

$$\begin{aligned} E_{10} = \frac{\partial^2 w}{\partial x^2}&\left[(\lambda+2\mu)\left({C_1}^2 - zC_1\right) - \frac{1}{4}\mu l^2(1-C_4)(1+C_4)\right] \\ &+ \frac{\partial^2 w}{\partial y^2}\left[\lambda C_1(-z+C_1) + \frac{1}{4}\mu l^2(1-C_4)(1+C_4)\right] \\ &+ \frac{\partial \varphi_x}{\partial x}\left[(\lambda+2\mu){C_1}^2 + \frac{1}{4}\mu l^2(1-C_4)^2\right] \\ &+ \frac{\partial \varphi_y}{\partial y}\left[\lambda{C_1}^2 - \frac{1}{4}\mu l^2(1-C_4)^2\right] \end{aligned} \quad (38)$$

$$E_{11} = \frac{\partial^2 w}{\partial y^2}\Big[\ (\lambda + 2\mu)\big({C_1}^2 - zC_1\big) - \tfrac{1}{4}\mu l^2(1 - C_4)(1 + C_4)\Big] + \frac{\partial^2 w}{\partial x^2}\Big[\lambda A_1(-z + C_1) + \tfrac{1}{4}\mu l^2(1 - C_4)(1 + C_4)\Big] + \frac{\partial \varphi_y}{\partial y}\Big[\ (\lambda + 2\mu){C_1}^2 + \tfrac{1}{4}\mu l^2(1 - C_4)^2\Big] + \frac{\partial \varphi_x}{\partial x}\Big[\lambda {C_1}^2 - \tfrac{1}{4}\mu l^2(1 - C_4)^2\Big] \quad (39)$$

$$E_{12} = \frac{\partial^2 w}{\partial x\,\partial y}\Big[-2\mu C_2 C_1 - \tfrac{1}{2}\mu l^2(1 - C_4)(1 + C_4)\Big] + \frac{\partial \varphi_x}{\partial y}\big[\mu {C_1}^2 + \mu l^2(1 - C_4)^2\big] + \frac{\partial \varphi_y}{\partial x}\Big[\mu {C_1}^2 - \tfrac{1}{2}\mu l^2(1 - C_4)^2\Big] \quad (40)$$

$$E_{13} = \frac{\partial^2 w}{\partial x\,\partial y}\Big[-2\mu C_2 C_1 - \tfrac{1}{2}\mu l^2(1 - C_4)(1 + C_4)\Big] + \frac{\partial \varphi_x}{\partial y}\Big[\mu {C_1}^2 - \tfrac{1}{2}\mu l^2(1 - C_4)^2\Big] + \frac{\partial \varphi_y}{\partial x}\big[\mu {C_1}^2 + \mu l^2(1 - C_4)^2\big] \quad (41)$$

$$E_{14} = \left(\frac{\partial w}{\partial x} + \varphi_x\right)\Big[\mu(1 - C_4)^2 + \tfrac{1}{4}\mu l^2 {C_5}^2\Big] + \left(\frac{\partial^2 \varphi_y}{\partial x \partial y} - \frac{\partial^2 \varphi_x}{\partial y^2}\right)\Big[\tfrac{1}{4}\mu l^2 C_5 C_1\Big] \quad (42)$$

$$E_{15} = \left(\frac{\partial w}{\partial y} + \varphi_y\right)\Big[\mu(1 - C_4)^2 + \tfrac{1}{4}\mu l^2 {C_5}^2\Big] + \left(\frac{\partial^2 \varphi_x}{\partial x \partial y} - \frac{\partial^2 \varphi_y}{\partial x^2}\right)\Big[\tfrac{1}{4}\mu l^2 C_5 C_1\Big] \quad (43)$$

The coefficients of C:

$$C_1 = z - \frac{4}{3}\left(\frac{1}{h}\right)^2 z^3 \quad (44)$$

$$C_2 = \frac{4}{3}\left(\frac{1}{h}\right)^2 z^3 \quad (45)$$

$$C_3 = \frac{4}{3}\left(\frac{1}{h}\right)^2 z^4 \quad (46)$$

$$C_4 = 4\left(\frac{z}{h}\right)^2 \quad (47)$$

$$C_5 = -8z\left(\frac{1}{h}\right)^2 \quad (48)$$

$$C_6 = \frac{4}{3}\left(\frac{1}{h}\right)^2 \quad (49)$$

$$C_7 = \mu\frac{h}{3} \quad (50)$$

$$C_8 = \mu\frac{h}{5} \quad (51)$$

$$C_9 = \frac{h^3}{252}(\lambda + 2\mu) \quad (52)$$

$$C_{10} = (\lambda + 2\mu)\frac{h^3}{60} \quad (53)$$

$$C_{11} = \mu\, l^2\frac{4}{3h} \quad (54)$$

$$C_{12} = \frac{1}{4}\mu\, l^2 h \quad (55)$$

$$I_i = \int_{-\frac{h}{2}}^{\frac{h}{2}} Z^i\, dz \;\; (i = 0,1,2,n-1,n,n+1,2n-4,2n-2,2n) \quad (56)$$

2.3 Buckling load

For a rectangular plate with length a, width b, and thickness h, under the axial forces (P_{xy}, P_y, P_x), the buckling force is obtained as shown in Eq. (57) [18, 19]:

$$P_x\frac{\partial^2 w}{\partial x^2} + 2P_{xy}\frac{\partial^2 w}{\partial x \partial y} + P_y\frac{\partial^2 w}{\partial y^2} = q(x,y) \quad (57)$$

Where P_x is the Axial force along the x-axis, P_y is the Axial force along the y axis, P_{xy} is the shear force in the xy plane, and q (x, y) is the out-of-plane force.

2.4 Virtual work equation

In this kind of problems the virtual work of three kinds of external forces are included in the solutions, if the middle-plane and the middle-perimeter of the plate are shown as Ω and Γ respectively, these virtual works are [20]:

1. The virtual work is done by the body forces, is applied on the volume V= Ω× (- h⁄2, h⁄2).
2. The virtual work is done by the surface tractions at the upper and lower surfaces (Ω).
3. The virtual work done by the shear tractions on the lateral surfaces, S= Γ× (- h⁄2, h⁄2).

If (f_x, f_y, f_z) is the body forces, (c_x, c_y, c_z) are the body couples, (q_x, q_y, q_z) are the forces acting on the Ω plane, (t_x, t_y, t_z) are the Cauchy's tractions and (S_x, S_y, S_z) are surface couples the Variations of the virtual work is expressed as:

$$\begin{aligned}\delta w = -\Big[\int_{\Omega} &(f_x\delta u + f_y\delta V + f_z\delta w + q_x\delta u + q_y\delta V + q_z\delta w + c_x\delta\theta_x \\ &+ c_y\,\delta\theta_y + c_z\delta\theta_z)\,dx\,dy + \int_{\Gamma}(t_x\delta u + t_y\delta V + t_z\delta w + s_x\theta_x \\ &+ s_y\delta\theta_y + s_z\delta\theta_z)d\Gamma\Big]\end{aligned} \quad (58)$$

Given that in this study only the external force q_z was applied, virtual work becomes:

$$\delta w = \int_0^a \int_0^b q(x,y)\delta w(x,y)dx\,dy \tag{59}$$

Finally using Hamilton's principle, it can be said that [21]:

$$\delta(U - w) = 0 \tag{60}$$

Where U is the strain energy and W is the work of external loads.

2.5 The final governing equations of the plate after applying the buckling and external forces

Using Hamilton's principle, Eq. (60), and the Eq. (57) – (59), the governing equations of the plate including the buckling and external forces are obtained as follows:

$$\left[\int_{-h/2}^{h/2}\left(\frac{\partial^2 E_1}{\partial x^2} - \frac{\partial E_4}{\partial x} + \frac{\partial^2 E_2}{\partial y^2} + \frac{\partial^2 E_3}{\partial x \partial y} - \frac{\partial E_5}{\partial y}\right)dz\right] + P_x\frac{\partial^2 w}{\partial x^2} + 2P_{xy}\frac{\partial^2 w}{\partial x \partial y} + P_y\frac{\partial^2 w}{\partial y^2} = q(x,y) \tag{61}$$

$$\int_{-h/2}^{h/2}\left(\frac{\partial^2 E_6}{\partial y^2} + \frac{\partial^2 E_9}{\partial x \partial y} - \frac{\partial E_{12}}{\partial y} - \frac{\partial E_{10}}{\partial x} + F_{14}\right)dz = 0 \tag{62}$$

$$\int_{-h/2}^{h/2}\left(\frac{\partial^2 E_7}{\partial x^2} - \frac{\partial E_{13}}{\partial x} + \frac{\partial^2 E_8}{\partial x \partial y} - \frac{\partial E_{11}}{\partial y} + E_{15}\right)dz = 0 \tag{63}$$

2.6. Obtaining the general equations of the third-order plate

Considering the following constants:

$$D_1 = 2C_{12} + l^2C_7 + \frac{1}{2}l^2C_8 + 2C_9 \tag{64}$$

$$D_2 = \frac{1}{2}D_1 = C_{12} + C_9 + \frac{1}{2}l^2C_7 + \frac{1}{4}l^2C_8 \tag{65}$$

$$D_3 = -\mu h + 2C_7 - C_8 - C_{11} \tag{66}$$

$$D_4 = C_9 - C_{10} + \frac{1}{4}l^2C_8 - C_{12} \tag{67}$$

$$D_5 = 3C_{12} - \frac{3}{2}l^2C_7 + \frac{3}{4}l^2C_8 - (\lambda+\mu)I_2 + 2(\lambda+\mu)C_6 I_4 - (\lambda+\mu){C_6}^2 I_6 \tag{68}$$

$$D_6 = -\mu I_2 + 2\mu C_6 I_4 - \mu {C_6}^2 I_6 - 4C_{12} + 2l^2C_7 - l^2C_8 \tag{69}$$

$$D_7 = \frac{1}{4}\mu l^2 I_2 - \frac{1}{2}\mu l^2 C_6 I_4 + \frac{1}{4}\mu l^2 {C_6}^2 I_6 \tag{70}$$

$$D_8 = -(\lambda+2\mu)I_2 + 2C_{10} - C_9 - C_{12} + \frac{1}{2}l^2C_7 - \frac{1}{4}l^2C_8 \tag{71}$$

$$D_9 = \frac{5}{4}l^2C_8 - \frac{3}{2}\mu l^2 {C_6}^2 I_4 - \frac{5}{2}l^2C_7 + 3C_{12} - (\lambda+\mu)I_2 - (\lambda+\mu){C_6}^2 I_6 + 2(\lambda+\mu)C_6 I_4 \tag{72}$$

$$D_{10} = 3l^2C_7 - \frac{3}{2}l^2C_8 + \frac{3}{2}\mu l^2 {C_6}^2 I_4 - \mu I_2 - \mu {C_6}^2 I_6 + 2\mu C_6 I_4 - 4C_{12} \tag{73}$$

The general governing equation of the Mindlin's plate will become:

$$D_1\frac{\partial^4 w}{\partial x^2\,\partial y^2}+D_2\frac{\partial^4 w}{\partial x^4}+D_2\frac{\partial^4 w}{\partial y^4}+D_3\frac{\partial^2 w}{\partial x^2}+D_3\frac{\partial^2 w}{\partial y^2}+D_4\frac{\partial^3 \varphi_x}{\partial x^3}+D_4\frac{\partial^3 \varphi_x}{\partial x\,\partial y^2}+D_4\frac{\partial^3 \varphi_y}{\partial y\,\partial x^2}+D_3\frac{\partial \varphi_x}{\partial x}+D_3\frac{\partial \varphi_y}{\partial y}+D_4\frac{\partial^3 \varphi_y}{\partial y^3}+P_x\frac{\partial^2 w}{\partial x^2}+2P_{xy}\frac{\partial^2 w}{\partial x\partial y}+P_y\frac{\partial^2 w}{\partial y^2}=q(x,y) \tag{74}$$

$$-D_4\frac{\partial^3 w}{\partial x\,\partial y^2}+D_5\frac{\partial^2 \varphi_y}{\partial y\,\partial x}+D_6\frac{\partial^2 \varphi_x}{\partial y^2}+D_7\frac{\partial^4 \varphi_y}{\partial x\,\partial y^3}-D_7\frac{\partial^4 \varphi_x}{\partial y^4}+D_7\frac{\partial^4 \varphi_y}{\partial y\,\partial x^3}-D_7\frac{\partial^4 \varphi_x}{\partial y^2\,\partial x^2}-D_3\frac{\partial w}{\partial x}-D_3\varphi_x-D_4\frac{\partial^3 w}{\partial x^3}+D_8\frac{\partial^2 \varphi_x}{\partial x^2}=0 \tag{75}$$

$$-D_4\frac{\partial^3 w}{\partial y\,\partial x^2}+D_9\frac{\partial^2 \varphi_x}{\partial y\,\partial x}+D_{10}\frac{\partial^2 \varphi_y}{\partial x^2}+D_7\frac{\partial^4 \varphi_y}{\partial x^4}+D_7\frac{\partial^4 \varphi_y}{\partial x^2\,\partial y^2}-D_7\frac{\partial^4 \varphi_x}{\partial y\,\partial x^3}-D_7\frac{\partial^4 \varphi_x}{\partial x\,\partial y^3}-D_4\frac{\partial^3 w}{\partial y^3}-D_3\frac{\partial w}{\partial y}-D_3\varphi_y+D_8\frac{\partial^2 \varphi_y}{\partial y^2}=0 \tag{76}$$

2.7 Solution of the governing equations using Navier's method

Navier's solution applies to the rectangular plates which have simply supported boundary conditions on all edges. Since the boundary conditions are spontaneously satisfied in this method, the unknown functions of the plate's mid-plane were assumed to be double trigonometric series [18, 20]:

$$W(x,y)=\sum_{m=1}^{\infty}\sum_{n=1}^{\infty}W_{mn}\sin\alpha x\sin\beta y \tag{77}$$

$$\varphi_x(x,y)=\sum_{m=1}^{\infty}\sum_{n=1}^{\infty}X_{mn}\cos\alpha x\sin\beta y \tag{78}$$

$$\varphi_y(x,y)=\sum_{m=1}^{\infty}\sum_{n=1}^{\infty}y_{mn}\sin\alpha x\cos\beta y \tag{79}$$

Moreover, the force can be calculated from the following relation:

$$q=\sum_{m=1}^{\infty}\sum_{n=1}^{\infty}Q_{mn}\sin\alpha x\sin\beta y \tag{80}$$

$$Q_{mn}=\frac{4}{ab}\int_0^a\int_0^b q(x,y)\sin\alpha x\sin\beta y\,dx\,dy \tag{81}$$

$$Q_{mn} = \begin{cases} q_0 & for\ sine\ Stress \\ \frac{16q_0}{mn\pi^2} & for\ uniform\ stress \\ \frac{4Q_0}{ab} & for\ point\ stress\ on\ the\ plate\ center \end{cases} \quad (82)$$

Where

$$\alpha = \frac{\pi m}{a}\ ,\ \beta = \frac{\pi n}{b}\ ,\ i = \sqrt{-1} \quad (83)$$

Furthermore, simply supported boundary conditions are satisfied by the Navier method based on the following equations:

$$\begin{matrix} x = 0 \text{ در} \\ x = a \end{matrix}' \begin{cases} w(0,y) = w(a,y) = \sum\sum w_{mn}\, sin\frac{m\pi}{a}\, x\, sin\frac{n\pi}{b}\, y = 0 \\ \varphi_y(0,y) = \varphi_y(a,y) = \sum\sum y_{mn}\, sin\frac{m\pi}{a}\, x\, cos\frac{n\pi}{b}\, y = 0 \end{cases} \quad (84)$$

$$\begin{matrix} y = 0 \text{ در} \\ y = b \end{matrix}' \begin{cases} w(x,0) = w(x,b) = \sum\sum w_{mn}\, sin\frac{m\pi}{a}\, x\, sin\frac{n\pi}{b}\, y = 0 \\ \varphi_x(x,0) = \varphi_x(x,b) = \sum\sum X_{mn}\, cos\frac{m\pi}{a}\, x\, sin\frac{n\pi}{b}\, y = 0 \end{cases} \quad (85)$$

2.8 The general equation matrix of third-order plate

After solving the governing equations and naming the coefficient of each variable:

$$R_1 = D_1\alpha^2\beta^2 + D_2\alpha^4 + D_2\beta^4 - D_3\alpha^2 - D_3\beta^2 - P_x\alpha^2 - P_y\beta^2 \quad (86)$$

$$R_2 = R_4 = D_4\alpha^3 + D_4\alpha\,\beta^2 - D_3\alpha \quad (87)$$

$$R_3 = R_7 = D_4\beta^3 + D_4\alpha^2\beta - D_3\beta \quad (88)$$

$$R_5 = -D_7\beta^4 - D_7\alpha^2\beta^2 - D_6\beta^2 - D_8\alpha^2 - D_3 \quad (89)$$

$$R_6 = D_7\alpha\beta^3 + D_7\alpha^3\beta - D_5\alpha\beta \quad (90)$$

$$R_8 = -D_7\alpha^3\beta - D_7\alpha\beta^3 - D_9\alpha\beta \quad (91)$$

$$R_9 = D_7\,\alpha^4 + D_7\alpha^2\beta^2 - D_{10}\alpha^2 - D_8\beta^2 - D_3 \quad (92)$$

Finally, the general equation matrix of the Mindlin's plate along with the auxiliary equations will be obtained as follows:

$$\begin{bmatrix} R_1 & R_2 & R_3 \\ R_4 & R_5 & R_6 \\ R_7 & R_8 & R_9 \end{bmatrix} \begin{bmatrix} w_{mn} \\ X_{mn} \\ y_{mn} \end{bmatrix} = \begin{bmatrix} Q_{mn} \\ 0 \\ 0 \end{bmatrix} \quad (93)$$

Various materials such as epoxy, graphene, copper, and so on can be considered as the plate's material. In this study, graphene is chosen as the plate's material. A single-layer graphene plate has

the following properties [21]:

$\mathrm{E} = 1.06TPa, \nu = 0.25\,, h = 0.34nm, \rho = 2250\,{}^{kg}/_{m^3}$

Also, the relationship between E, μ, and ν can be expressed as:

$$\lambda = \frac{\nu E}{(1+\nu)(1-2\nu)} \quad ,\mu = \frac{E}{2(1+\nu)} \tag{94}$$

Where E is the Young modulus, and μ and λ are the Lame coefficients [22]. Then, $\mathrm{q} = {}^{1\mathrm{N}}/_{\mathrm{m}^2}$ is considered as the stress amount.

3. Results and Discussion

Results were obtained using a computational program coded in MATLAB software. The plate's dimensional parameters are chosen as follows:

a: plate's length

b: plate's width

h: plate's thickness

l: material length scale parameter

Table 1 shows that the value of dimensionless bending of third-order nanoplate under the sinusoidal load is less than that of the uniform surface traction. The dimensionless bending value increases by increasing the aspect ratio of the plate. Besides, the aforementioned value decreases by increasing the length scale parameter to thickness ratio.

Figure 1 presents the bending value of different nanoplates under uniform surface traction for different length-to-width ratios. According to Fig. 1, the bending value is the lowest for the Kirchhoff nanoplate and the highest for the third-order nanoplate.

Table 2 represents the bending value of the third-order nanoplate subjected to uniform surface traction for different length to width and parameter length scale to thickness ratios. The bending value of the plate decreases by increasing the length parameter to thickness ratio. In addition, increasing the aspect ratio of the plate leads to higher bending values.

Figure 2 depicts the bending value of the third-order nanoplate under sinusoidal loading for different length to width and length scale parameter to thickness ratios. The figure shows that the bending value of the plate declines by increasing the length parameter to thickness ratios. Furthermore, it was observed that increasing the aspect ratio of the plate leads to higher bending values.

Figure 3 exhibits the bending contours of the third-order nanoplate under uniform_surface traction. According to the results, the maximum bending value occurs at the center of the plate.

Figure 4 presents the critical buckling load of third-order nanoplate subjected to a biaxial loading in x and y directions. This value increases by increasing the ratio of length scale parameter to thickness and decreases by increasing the ratio of length to thickness.

Table 3 shows that the critical buckling load of the third-order nanoplate under uniaxial loading in x-direction increases by increasing the length scale parameter to thickness ratio and declines with

increasing the length to the thickness ratio. In addition, by comparing the results of Table 3 and Fig. 4 it can be found that the critical buckling load in the uniaxial loading yields greater values than that of the biaxial loading.

Table 4 lists the dimensionless critical buckling loads of different nanoplates subjected to biaxial loadings in x and y directions. Where an increase in length to thickness ratio leads to different behaviors as follows:

- The dimensionless critical load increases by increasing the length to thickness ratio of Mindlin nanoplate.
- The dimensionless critical load decreases slightly by increasing the length to thickness ratio of the third- and fifth-order shear nanoplates.
- The dimensionless critical load remains unchanged while increasing the length to thickness ratio of the Kirchhoff nanoplate.

Table 1. Comparison of dimensionless bending of third order nanoplate under sinusoidal and uniform surface traction for various length to width ratio (a / h = 30 and q = 1e-18 N / nm ^ 2)

a/b	*l/h*							
	0		0.5		1		2	
	Uniform load	Sinusoidal load	Uniform load	Sinusoidal load	Uniform load	Sinusoidal load	Uniform load	Sinusoidal load
1	1.0000	1.0000	0.49874	0.49858	0.19922	0.19912	0.05856	0.05852
1.5	1.0000	1.0000	0.49911	0.49883	0.19945	0.19927	0.05864	0.05858
2	1.0000	1.0000	0.49923	0.49895	0.19952	0.19935	0.05866	0.05860

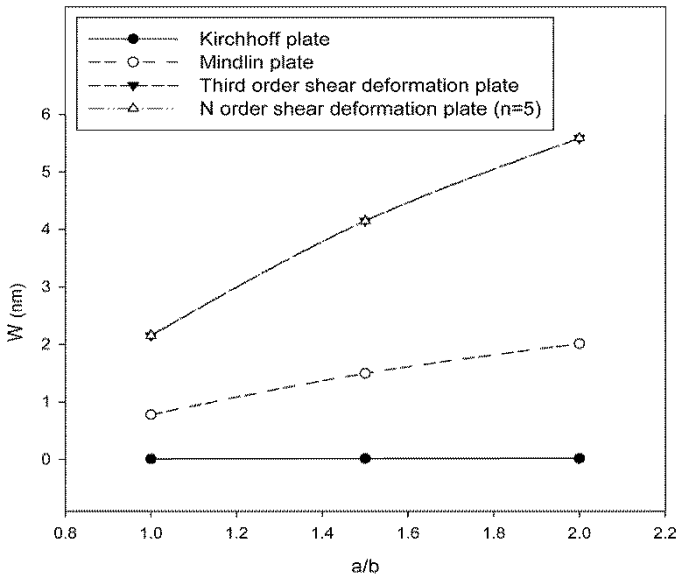

Figure 1. Comparison of dimensionless bending of different nanoplates under uniform surface traction for various length to width ratio (a/h=30 and q=1e-18 N/nm^2, l/h=1)

Table 2. Bending values of third-order nanoplate under uniform surface traction for various length to width and length parameter to thickness ratios (q=1e-18 N/nm^2 and a/h=30)

a/b	*l/h*			
	0	0.5	1	2
1	10.7837	5.3783	2.1483	0.6315
1.5	20.7713	10.3671	4.1428	1.2179
2	28.0010	13.9789	5.5868	1.6426

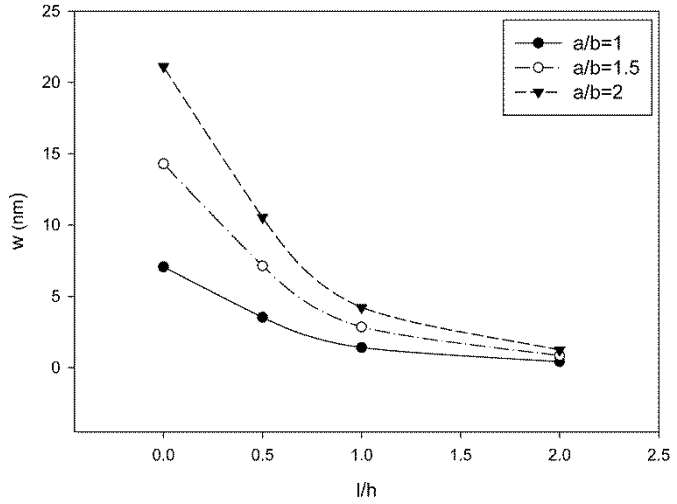

Figure 2. Bending values of third-order nanoplate under Sinusoidal stress for various length to width and length parameter to thickness ratios (q=1e-18 N/nm^2 and a/h=30)

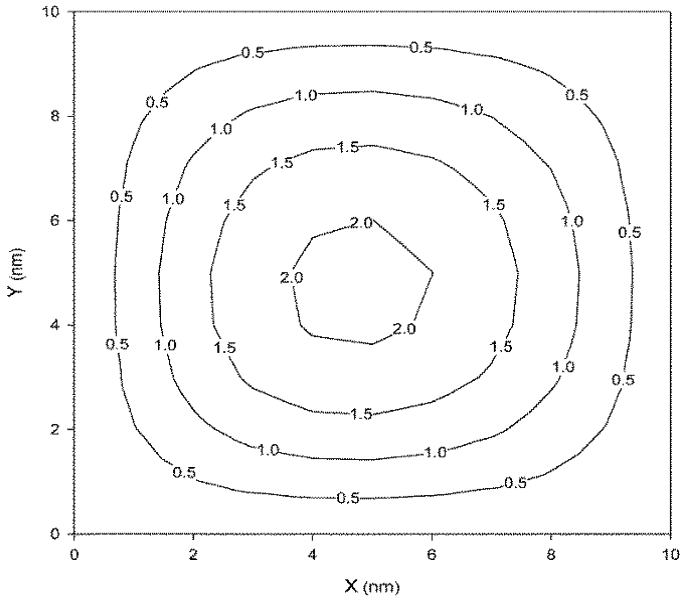

Figure 3. Bending contours of the third order nanoplate (a/h=30, q=1e-18 N/nm^2, and a/b=1, l/h=1)

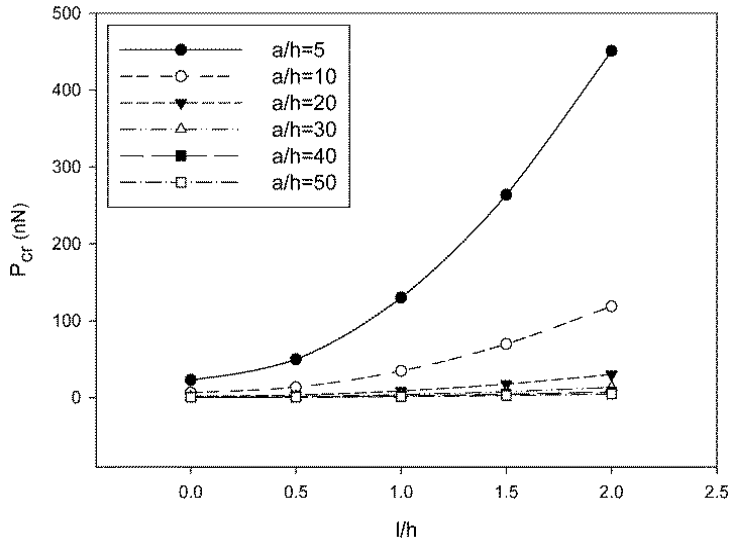

Figure 4. Comparison of the critical buckling load of third-order nanoplate under biaxial loading in x- y direction for various length to width and length to thickness ratios (a / b = 1)

Table 3. Comparison of the critical buckling load of third-order nanoplate under the uniaxial loading in x-direction for various length to width and length parameter to thickness ratios (a / b = 1)

a/h	*l/h*				
	0	0.5	1	1.5	2
5	46.0378	99.6890	260.2116	527.5054	901.6352
10	13.4331	27.4598	69.4801	139.4830	237.4772
20	3.5051	7.0497	17.6789	35.3919	60.1893
30	1.5706	3.1490	7.8834	15.7736	26.8197
40	0.8860	1.7744	4.4396	8.8813	15.0997
50	0.5678	1.1366	2.8429	5.6867	9.6679

Table 4. Comparison of the dimensionless critical buckling load of third-order nanoplate under the biaxial loading in x-y direction for various length to width and length to thickness ratios (a / b = 1, I/h=1)

a/h	*Kirchhoff plate*	*Mindlin plate*	*Third-order shear deformation plate*	*N order shear deformation plate (n=5)*
5	5.0000	10.1594	5.6521	5.6937
10	5.0000	12.8101	5.1723	5.1826
20	5.0000	13.6820	5.0437	5.0463
30	5.0000	13.8568	5.0195	5.0206
40	5.0000	13.9191	5.0110	5.0116
50	5.0000	13.9481	5.0070	5.0074

4. Conclusion

In this study, the bending and buckling of a third-order nanoplate were investigated using the modified couple stress theory. Based on the obtained results presented in the tables and figures, the dimensionless bending value of the third-order nanoplate under the sinusoidal load is less than that of the uniform surface traction. Besides, increasing the length parameter to the thickness ratio led to a lower dimensionless bending value of the nanoplate. Furthermore, the value of dimensionless

bending increases with increasing the aspect ratio of the plate. The bending results showed that the Kirchhoff nanoplate has the lowest and the third-order nanoplate has the highest bending values.
The critical buckling load value of the third-order nanoplate under uniaxial loading in x-direction increases with increasing the ratio of the length scale parameter to the thickness of the nanoplate, while it decreases by increasing the length to thickness ratio. moreover, it was found that the critical buckling load under uniaxial loading is greater than the critical buckling load under biaxial loading.

5. References

[1] Thanh, C.-L., Tran, L. V., Vu-Huu, T. and Abdel-Wahab, M. 2019. The size-dependent thermal bending and buckling analyses of composite laminate microplate based on new modified couple stress theory and isogeometric analysis. Computer Methods in Applied Mechanics and Engineering. 350: 337-361.

[2] Sladek, V., Sladek, J., Repka, M. and Sator, L. 2020. FGM micro/nano-plates within modified couple stress elasticity. Composite Structures. 245: 112294.

[3] Al-Shewailiah, D. M. R. and Al-Shujairi, M. A. 2021. Static bending of functionally graded single-walled carbon nanotube conjunction with modified couple stress theory. Materials Today: Proceedings.

[4] Yang, Y., Hu, Z.-L. and Li, X.-F. 2021. Axisymmetric bending and vibration of circular nanoplates with surface stresses. Thin-Walled Structures. 166: 108086.

[5] Aghababaei, R. and Reddy, J.N. 2009. Nonlocal third-order shear deformation plate theory with application to bending and vibration of plates. Journal of Sound and Vibration. 326: 277-289.

[6] Jung, W.Y., Han, S.C. and Park, W.T. 2014. A modified couple stress theory for buckling analysis of S-FGM nanoplates embedded in Pasternak elastic medium. Composites Part B: Engineering. 60: 746-756.

[7] Shafiei, Z., Sarrami-Foroushani, S., Azhari, F. and Azhari, M. 2020. Application of modified couple-stress theory to stability and free vibration analysis of single and multi-layered graphene sheets. Aerospace Science and Technology. 98: 105652.

[8] Wu, C.-P. and Hu, H.-X. 2021. A unified size-dependent plate theory for static bending and free vibration analyses of micro- and nano-scale plates based on the consistent couple stress theory. Mechanics of Materials. 162: 104085.

[9] Haghshenas, A. and Shahrajabian, H. 2021. The mechanical properties of PA6/NBR/clay/CaCO3 hybrid nanocomposites. Journal of Modern Processes in Manufacturing and Production. 10(1): 19-30.

[10] Ameen, S., Akhtar, M. S. and Shin, H. 2020. Graphene Production and Application. IntechOpen. https://doi.org/10.5772/intechopen.83309

[11] Sun, Y., Sun, M. and Xie,D. 2018. Graphene Electronic Devices. Academic Press.

[12] Yang, F., Chong, A.C.M., Lam, D.C.C. and Tong, P. 2002. Couple stress Based Strain gradient theory for elasticity. Int.J.Solids Struct. 39: 2731–2743.

[13] Toupin, R.A. 1962. Elastic materials with couple stresses. Arch.Rational Mech.Anal. 11: 385–414.

[14] Mindlin, R.D. and Tiersten, H.F. 1962. Effects of couple-stresses in linear elasticity. Arch. Rational Mech. Anal. 11: 415–448.

[15] Koiter, W.T. 1964. Couple stresses in the theory of elasticity. I and II.Proc .K. Ned. Akad .Wet.(B) 67: 17–44.

[16] Mindlin, R.D. 1964. Micro-structure in linear elasticity. Arch.RationalMech.Anal. 16: 51–78.

[17] Tsiatas, G.C. 2009. A new kirchhoff model based on a modified couple stress theory. International Journal of solids and structures. 46: 2757-2764.

[18] Wang, B., Zhou, S., Zhao, J. and Chen, X. 2011. A size-dependent kirchhoff micro-plate model based on strain gradient elasticity theory. European Journal of mechanics A/Solids. 30: 517-524.

[19] Farajpour, A., Shahidi, A.R., Mohammadi, M. and Mahzoon, M. 2012. Buckling of orthotropic micro/nanoscale plates under linearly varying in-plate load via nonlocal continuum mechanics. Composite Structures. 94: 1605-1615.

[20] Tai, T. and HoChoi, D. 2013. size-dependent functionally graded kirchhoff and mindlin plate theory based on a modified couple stress theory. Composite Structures. 95: 142-153.

[21] Akgoz, B. and Civalek, O. 2012. Free vibration analysis for single –layered graphene sheets in an elastic matrix via modified couple stress theory. materials and design. 42: 164-171.

[22] Roque, C.M.C., Ferreira, A.J.M. and Reddy, J.N. 2013. Analysis of mindlin micro plates with a modified couple stress theory and meshlessmethod. Applied Mathematical Modeling. 37: 4626-4633.